Photodynamic Therapy



In Situ Disinfection through Photoinspired Radical Oxygen Species Storage and Thermal-Triggered Release from Black Phosphorous with Strengthened Chemical Stability

Lei Tan, Jun Li, Xiangmei Liu, Zhenduo Cui, Xianjin Yang, Kelvin Wai Kwok Yeung, Haobo Pan, Yufeng Zheng, Xianbao Wang, and Shuilin Wu*

Photodynamic therapy (PDT) utilizing light-induced reactive oxygen species (ROS) is a promising alternative to combat antibiotic-resistant bacteria and biofilm. However, the photosensitizer (PS)-modified surface only exhibits antibacterial properties in the presence of light. It is known that extended photoirradiation may lead to phototoxicity and tissue hypoxia, which greatly limits PDT efficiency, while ambient pathogens also have the opportunity to attach to biorelevant surfaces in medical facilities without light. Here, an antimicrobial film composed of black phosphorus nanosheets (BPSs) and poly (4-pyridonemethylstyrene) endoperoxide (PPMS-EPO) to control the storage and release of ROS reversibly is introduced. BPS, as a biocompatible PS, can produce high singlet oxygen under the irradiation of visible light of 660 nm, which can be stably stored in PPMS-EPO. The ROS can be gradually thermally released in the dark. In vitro antibacterial studies demonstrate that the PPMS-EPO/BPS film exhibits a rapid disinfection ability with antibacterial rate of 99.3% against Escherichia coli and 99.2% against Staphylococcus aureus after 10 min of irradiation. Even without light, the corresponding antibacterial rate reaches 76.5% and 69.7%, respectively. In addition, incorporating PPMS significantly improves the chemical stability of the BPS.

1. Introduction

The colonization of pathogens on surfaces in medical facilities often leads to infectious diseases or even death, afflicting millions of people annually. The new or re-emergence of infectious diseases has caused over 13 million deaths annually in the 21st century.[1] To address this issue, new types of antibiotics and various kinds of antibacterial agents such as metal ions, metal nanoparticles, and biocides have been successfully used to prevent pathogen colonization.[2] Abuse of antibiotics has contributed to the problem of severe antibiotic resistance and emergence of superbacteria. Bacteria in the presence of antibiotics can reportedly develop antibiotic resistance in less than two weeks, suggesting that the rate of antibiotic discovery cannot keep up with pathogens' generation of antibiotic resistance.[3] In addition, antibiotic abuse often impairs the immune

Dr. L. Tan, Dr. J. Li, Dr. X. M. Liu, Prof. X. B. Wang, Prof. S. L. Wu
Hubei Collaborative Innovation Center for Advanced Organic Chemical Materials
Ministry-of-Education Key Laboratory for the Green Preparation and Application of Functional Materials
Hubei Key Laboratory of Polymer Materials
School of Materials Science & Engineering
Hubei University
Wuhan 430062, China
E-mail: shuilin.wu@gmail.com, shuilinwu@tju.edu.cn
Prof. Z. D. Cui, Prof. X. J. Yang, Prof. S. L. Wu
School of Materials Science & Engineering
Tianjin University
Tianjin 300072, China

Pokfulam, Hong Kong 999077, China
Prof. H. B. Pan
Center for Human Tissues and Organs Degeneration
Shenzhen Institutes of Advanced Technology
Chinese Academy of Sciences
Shenzhen 518055, China
Prof. Y. F. Zheng
China State Key Laboratory for Turbulence and Complex System
and Department of Materials Science and Engineering
College of Engineering
Peking University
Beijing 100871, China

Department of Orthopaedics & Traumatology

The ORCID identification number(s) for the author(s) of this article can be found under https://doi.org/10.1002/smll.201703197.

DOI: 10.1002/smll.201703197

Prof. K. W. K. Yeung

Li Ka Shing Faculty of Medicine

The University of Hong Kong





system's congenital ability to resist outside invasions.^[4] In this case, various antibacterial agents such as metal ions, metal nanoparticles, and biocides were successfully used. However, these antibacterial agents, such as silver nanoparticles, still show unacceptably toxic tissue effects on human health and the environment. [5] Besides cancer treatment, [6] photodynamic therapy (PDT) is considered a promising alternative to combat antibiotic-resistant bacteria and biofilm.[7] The pathogens can be killed by reactive oxygen species (ROS) such as singlet oxygen that are generated from a photosensitizer (PS) under light through energy or electron transfer to molecular oxygen. [8] As strong oxidants, ROS can disinfect pathogens by reacting with their essential macromolecules such as DNA, RNA, and pathogenic proteins, damaging the cell membrane and cell wall and causing the pathogen's death. [9] Although PDT is controllable compared to other antibacterial agents, there are still problems that should be addressed. In general, the PS only produces ROS and exhibits antibacterial properties in the presence of light. However, prolonged irradiation may result in phototoxicity and tissue hypoxia, which greatly limit PDT efficiency.[10] It is also uneconomical and shortens the light source's lifetime. When the light source is removed, the ambient pathogens also have the opportunity to attach to biorelevant surfaces, which are still vulnerable to pathogen infection. Medical facilities only sterilize prior to use; sterilization cannot be maintained during use. Endowing biorelevant surfaces with self-disinfection abilities in the absence of light is key to addressing these issues. It is known that 2-pyridone can trap singlet oxygen and produce endoperoxide. The endoperoxides of 2-pyridone derivatives are recognized as a promising chemical singlet oxygen source as they can be stored stably in a freezer more than one year and then release the singlet oxygen under thermal decomposition without side reactions.[11] In fact, 2-pyridone endoperoxides have been used to improve PDT efficiency in cancer treatment.^[12] Therefore. by combining PS and 2-pyridone derivatives, the goal of eradicating pathogens from biorelevant surfaces can be realized with or without irradiation. Medical facilities would benefit from this innovation because surgical instruments, medical catheters, and implant materials could rapidly kill pathogens in situ and prevent infection during use. Joint prosthesis and dental implants are especially vulnerable to the risk of biofilm infections. If the initial pathogens attached to the implants could be eliminated, the probability of biofilm formation could be greatly reduced. Furthermore, inflammation usually leads to pyrexia, which accelerates the release of singlet oxygen from the endoperoxide (EPO) and kills pathogenic bacteria rapidly.

Black phosphorus (BP), a newly developed 2D material, is a metal-free semiconductor with a layer-dependent direct bandgap, which can be varied from 0.3 eV for bulk to 2.0 eV for a single layer, indicating broad absorption across the ultraviolet and infrared regions.^[13] Recently, BP nanosheets (BPSs) have shown excellent PDT performance in cancer treatments, possibly due to its high singlet oxygen generation ability and robust biocompatibility.^[14] The instability of BP, however, limits its potential in biomedical applications. Significant efforts have been made to improve the stability of BP through surface coordination, tellurium doping, chemical modification,

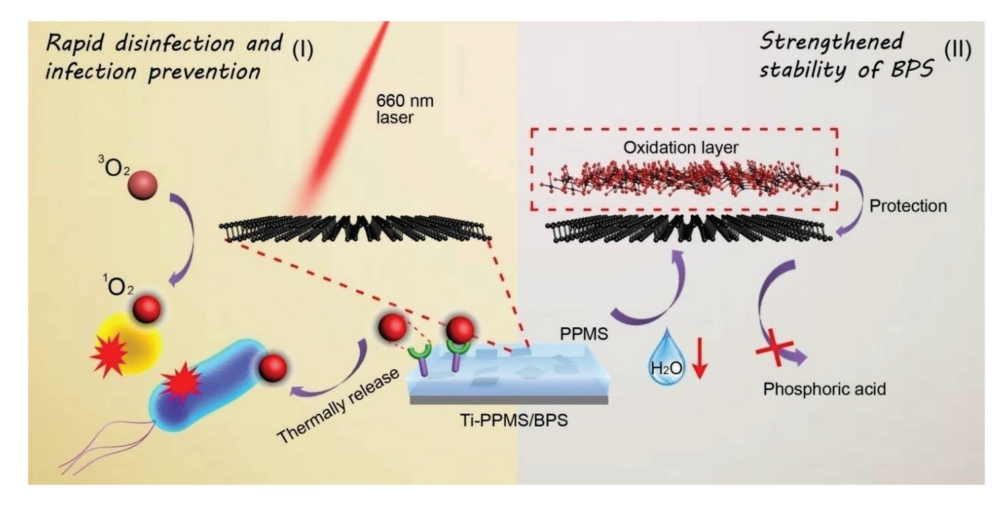
and noncovalent functionalization. [15] BP exhibits poor stability in ambient because BP tends to react with adsorbed water or oxygen on the surface. [16] The first stage of BP is the formation of P_xO_y . Although the oxidation layer can slow dawn the degradation of BP to a certain extent, however, the P_xO_y can continue to react with water to form phosphoric acid. The phosphoric acid will be lost along with water and lead to the further degradation of the underneath BP. [17] Thus, if the amount of water adsorbed by the BP could be reduced and the transformation from P_xO_y to phosphoric acid can be suppressed, BP's stability may improve.

Herein, we for the first time developed a surface system to achieve the storage and release of ROS for rapid disinfection and infection prevention with strengthened chemical stability of BPS, which was schematically illustrated in Scheme 1. Briefly, BPS was used as a photosensitizer to generate singlet oxygen for antibacterial application, while poly (4-pyridonemethylstyrene) (PPMS) was composited with the BPS to store the singlet oxygen. This hybrid system can generate singlet oxygen in the presence and absence of light (660 nm, 0.5 W cm⁻²). Antibacterial experiments in vitro and in vivo showed that the PPMS-EPO/BPS film exhibited excellent antibacterial performance in the presence and absence of light. The stability of BP was significantly improved due to the coprotection of hydrophobic PPMS and oxidation layer on the surface of BPS, which could prevent the further degradation of the underneath BP.

2. Results and Discussion

2.1. Morphology and Characterization

BPS was prepared by liquid phase exfoliation. Although BP can be efficiently exfoliated using amide solvents such as N-methyl-2-pyrrolidone and N-cyclohexyl-2-pyrrolidone, the adsorption of these solvents on the surface of BPS are hard to remove completely.[16] Therefore, the BP was exfoliated with a water exfoliation strategy to obtain a clean surface, which benefits the combination of BPS and PPMS. The morphology of the BPS was observed through a transmission electron microscopy (TEM). The exfoliated BPS looked transparent under the electron beam, suggesting the BPS was sufficiently thin (Figure 1a). The average size of BP and PPMS/BPS were measured to be 531 and 588 nm, respectively (Figure 1b). An atomic force microscopy (AFM) was employed to measure the topographic morphology and thickness of the BPS (Figure 1c,d). The surface of the BPS was flat, suggesting that the exfoliation had not degraded the BPS. Form the X-ray photoelectron spectra (XPS) measurement, the weak peak around 134 eV of exfoliated BPS was the signal of P_xO_y , indicating the minor degradation on the surface of the BPS (Figure S3, Supporting Information). A cross-sectional analysis showed that the BPS heights of 4.2 and 4.5 nm corresponded to BPS with 7 layers. [16] This result provided additional proof that the BP had been successfully exfoliated. From the SEM image of the cross section of PPMS-EPO/BPS on titanium plate, the thickness of film was around 22 µm (Figure 1e). After the BPS and PPMS were combined, the surface of PPMS/BPS film was flat, and the flake



Scheme 1. Schematic that shows the PPMS/BPS inactivating bacteria through generating singlet oxygen (¹O₂) in the presence and absence of light, and the stability of BPS can be improved by PPMS.

shape of BPS was not observed. This result meant that the BPS was completely encapsulated and uniformly distributed throughout the PPMS. The hydrophobic polymer acted as a protective shell for the BPS and kept them from being exposed to the external environment (Figure 1f). An X-ray diffraction (XRD) analysis was employed to confirm the crystalline structures of the BPS and PPMS/BPS films. Bragg peaks of (020), (040), and (060) were observed in the XRD pattern of both the BPS and PPMS/BPS films, which were matched to the orthorhombic phase.^[18] The results also implied that the BPS

within both films remained flatly restacked on the titanium (Ti) substrates (Figure 1g).^[19] The formation of the PPMS/BPS film was also examined by FTIR spectroscopy (Figure 1h). The weak absorption band at 1086 cm⁻¹ was attributed to the P—O stretching vibration of BPS, suggesting that a few oxidations occurred on the surface of BPS. After the combination with PPMS, the absorption band at 1660 cm⁻¹ showed a C=O bond of N-substituted 2-pyridone, the typical broad peaks at 2915 and 2844 cm⁻¹ (—CH₂) and peaks from 667 to 1255 cm⁻¹ (C—H) were from the flexural vibration of the benzene or pyridone

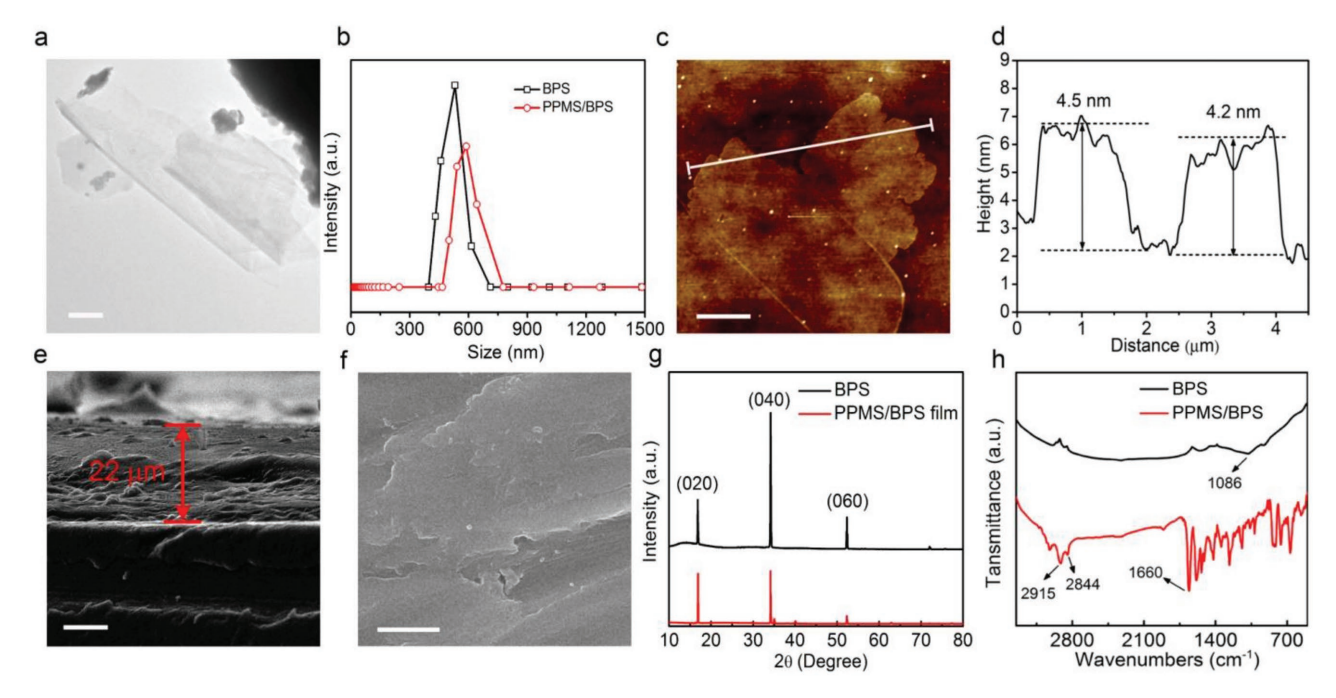


Figure 1. Morphology and structure characterization of BPS and PPMS/BPS. a) TEM image of BPS exfoliated in water (scale bar, 100 nm). b) Size distributions of BPS and PPMS/BPS in dichloromethane solution. c) AFM image shows the flat features of BPS (scale bar, 1 μ m). d) Height profiles along the white lines in (c). e) SEM image shows the thickness of PPMS/BPS on Ti substrate (scale bar, 10 μ m). f) SEM image shows the flat morphology of PPMS/BPS film on Ti substrate (scale bar, 1 μ m). g) The XRD characterizations of BPS and PPMS/BPS films are matched to the orthorhombic phase. h) FTIR measurement shows the successful combination of BPS and PPMS.

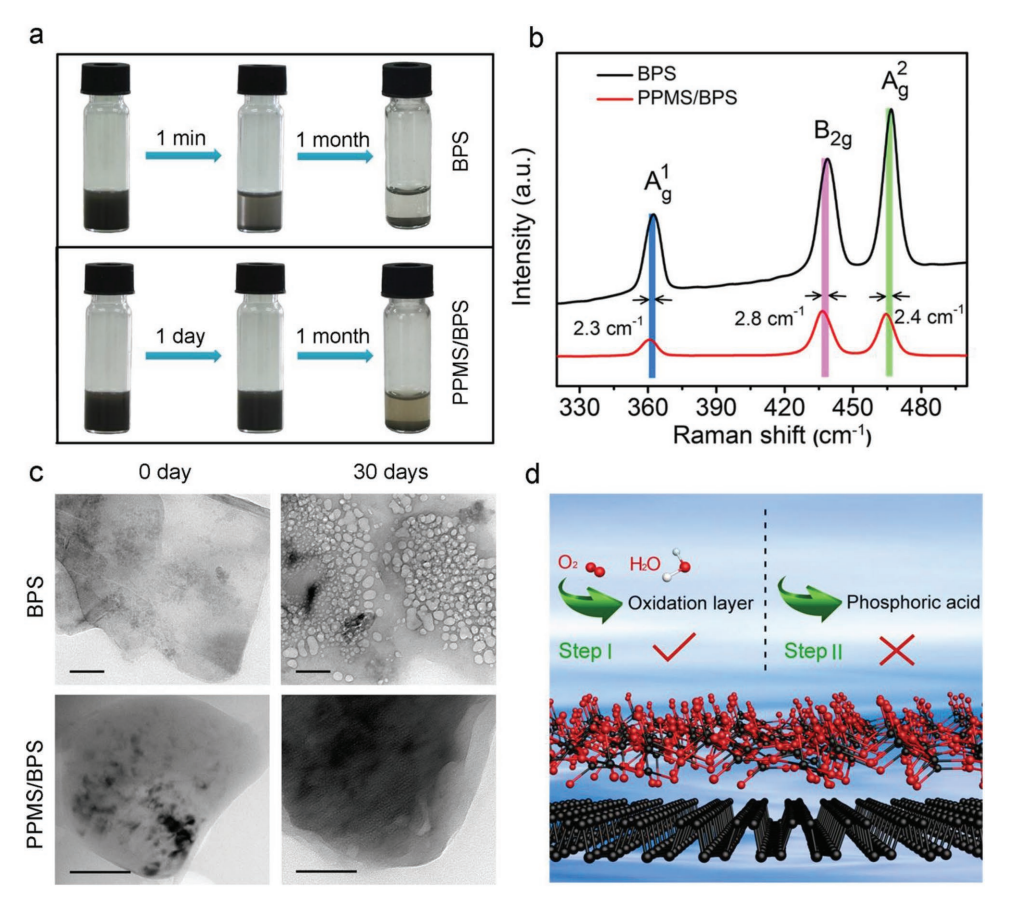


Figure 2. Degradation performance. a) Photograph of BPS and PPMS/BPS dispersed in DCM shows the long time suspension of PPMS/BPS. b) Raman spectra show the A_g^1 , B_{2g} , and A_g^2 modes of PPMS/BPS were redshifted compared to BPS. c) TEM images of BPS and PPMS/BPS show the degradation state of surface topography before and after one month (scale bars, 100 nm). d) Schematic illustration of the improved stability of BPS by PPMS.

ring, indicating that the PPMS was combined with the BPS successfully.

2.2. Stability Performance of PPMS/BPS

Before investigating the stability of the PPMS/BPS film, we first investigated the dispersion of BPS in a PPMS solution. Using ultrasound, the BPS (100 μg mL⁻¹) was fully dispersed into pure dichloromethane (DCM) and a PPMS (20 mg mL⁻¹) solution of DCM. Then, the states of the two samples were photographed (Figure 2a). For the DCM solution of BPS, most of the BPS precipitated after 1 min, indicating that the DCM could disperse a small amount of BPS for a short time. However, a month later, the supernate of the sample was thoroughly clear, suggesting that the interaction between the BPS and the DCM solvent was too weak to maintain the state of suspension for an extended period. In contrast, even though the PPMS/BPS group sample was photographed after one day, the supernate was still turbid and in an unchanged state compared to the initial time. A month later, although most of the BPS had precipitated, the grey color of supernate could still be observed, which may be attributed to the strong

affinity between the PPMS and a certain amount of the BPS. This phenomenon implied that the PPMS chain could adsorb onto the surface of the exfoliated BPS in a DCM solvent. More specifically, the life spans of suspensions were determined by the reaggregation rate of dispersed flakes, while the interactive energy between the salvation shells and flakes controlled the reaggregation rate. For the DCM, the cohesive force between the DMC and the BPS was very weak because the energy barrier was too low, resulting in the difficult dispersion of the BPS.^[20] Introducing PPMS significantly prolonged the lifespan of the suspension, suggesting that the strong cohesive force between the PPMS and the BPS makes it difficult to overcome the energy barrier and induce aggregation. The zeta potential of the BPS and PPMS/BPS in deionized water were measured to be -26.9 and 2.3 mV, respectively, indicating the existent of electrostatic interaction between BPS and PPMS (Figure S4, Supporting Information). Thus, we hypothesized that the PPMS could protect the BPS from degradation once the PPMS/BPS film formed on the substrate. Consequently, this hydrophobic polymer functioned as a protective shell around the BPS and largely prevented it from degrading. To investigate the effect of the PPMS toward the BPS, a Raman scattering was performed to characterize





the BPS and PPMS/BPS films (Figure 2b). The BPS showed three prominent Raman peaks due to one out-of-plane phonon mode A¹_g at 362.3 cm⁻¹ and two in-plane modes B_{2g} and A²_g at 438.8 and 466.9 cm⁻¹, respectively. Compared to the BPS films, the A_g^1 , B_{2g} , and A_g^2 modes of the PPMS/BPS films were redshifted by about 2.3, 2.8, and 2.4 cm⁻¹, respectively. The strong cohesive force between PPMS and BPS might hinder the oscillation of P atoms to some extent, thus lowering the Raman scattering energy and redshifting the Raman peaks.[15a] This result further proved the existence of a strong interaction between the PPMS and the BPS. To more directly observe the degradation of BPS and PPMS/BPS. The surface topography of BPS and PPMS/BPS was investigated through TEM. The mapping analyses of PPMS/BPS revealed the presence of N, O, and P element in the sample, proving that the BPS was successfully encapsulated by PPMS (Figure S5, Supporting Information). From Figure 2c, the degradation bubbles were spread on the surface of BPS after one month. However, the degradation degree of PPMS/BPS was significantly suppressed. We could find that tiny bubbles appeared on the surface of PPMS/BPS, which was the oxidation layer of BPS. No appearance of big bubbles proved that the underneath BPS in PPMS/BPS film did not continue to degradation. The improved stability of BP was attributed to the coprotection of hydrophobic PPMS and oxidation layer on the surface of BPS, which can prevent the further degradation of the underneath of BP. Besides, since phosphoric acid will be lost along with water and lead to the further degradation of the underneath BP, the strong cohesive force between the hydrophobic PPMS and BPS can prevent the transformation from P_xO_y to phosphoric acid by reducing the contact opportunity of oxidation layer with water (Figure 2d).

2.3. Storage and Release of Singlet Oxygen

The PPMS was able not only to protect the BPS but also to store the singlet oxygen (1O2) produced from the BPS and then release it under thermal decomposition. The operation mechanism for the reversible singlet oxygen storage and release of the PPMS is shown in Figure 3a. When irradiated by the 660 nm light (0.5 W cm⁻²), the BPS in the PPMS/BPS generated singlet oxygen, and some of the singlet oxygen was stored in the PMMS in the form of PPMS-EPO. When the irradiation is turned off, the PPMS-EPO can regenerate PPMS and singlet oxygen through thermal decomposition. To investigate the reversible transformation between the pyridone and the endoperoxide, the structure were determined using ¹H nuclear magnetic resonance (NMR). From the partial ¹H NMR data in Figure 3b, the peak at $\delta = 6.51$ ppm was attributed to the proton on the pyridone ring. After irradiating the CDCl₃ solution of the PPMS/BPS with 660 nm of light, the arising peaks at $\delta = 6.74$, 6.30, and 5.89 (endoperoxide ring) and δ = 4.82 ppm (*N*-CH₂) were attributed to the proton of endoperoxide, indicating that the PPMS was partially transformed to PPMS-EPO successfully. We calculated from the integral area of ¹H NMR spectra of PMMS-EPO, about 33% of the PPMS transformed to PPMS-EPO. When the CDCl₃ solution of the PPMS-EPO was placed at 37 °C in the dark for 24 h, the ¹H NMR spectrum of the PPMS-EPO changed back to the initial structure reversibly. This outcome indicated that the PPMS could store the singlet oxygen generated from the BP via their reaction with the pyridone groups and subsequently release it by thermal decomposition. An XPS measurement was employed to further check the reversible transformation between the PPMS/BPS and PPMS-EPO/BPS films. After irradiation, the element ratio of O: N = 2.0 in the PPMS-EPO/BPS film was increased compared to the O: N = 1.5 of the PPMS/ BPS, which was attributed to the formation of endoperoxide (Figure S6a, Supporting Information). In the high resolution of C1s spectra of the PPMS/BPS and PPMS-EPO/BPS films (Figure S7a,b, Supporting Information), the C-C, C=C, C-N, and O=C-N at 284.6, 284.1, 285.7, and 287.2 eV proved the structure of the PPMS, and the C-O at 287.0 eV further indicated the formation of endoperoxide. The P signal of the PPMS/BPS film was not detected, which could be explained by the fact that the shell thickness of the polymer around the BPS was greater than the detection depth of the XPS (around 10 nm). This thickness might also contribute to the protection of the BPS (Figure S6b, Supporting Information).

The generation of singlet oxygen from the BPS and the PPMS-EPO could be evaluated by a probe molecule such as 1, 3-diphenylisobenzofuran (DPBF). DPBF can react with singlet oxygen through Diels-Alder 1, 4-cycloaddition, [14] exhibiting a decrease of UV absorption at about 415 nm. Figure 3c shows the photocatalystic ability of the PPMS/BPS; the absorption at 415 nm decreased gradually as the irradiation time increased in air at 20 °C (660 nm light, 0.5 W cm⁻²), indicating that the DPBF was decomposed by singlet oxygen generated from the PPMS/BPS. As a control, the absorption of the DPBF showed negligible change with or without irradiation (Figure 3c and Figure S8b, Supporting Information). When a very weak stream of oxygen was bubbled through the sample at 20 °C, the ultimate decomposition degree of the DPBF ($I/I_0 = 0.61$) was greater than the condition in the air $(I/I_0 = 0.68)$, suggesting that increasing the oxygen content contributed to the generation of singlet oxygen. It should be noted that the decomposition degree of the DPBF was even lower within the first 20 min, which might result from the enhanced storage of singlet oxygen in the form of PPMS-EPO (Figure 3d). The singlet oxygen released from the PMMS-EPO was operated by placing the sample in the dark at 37 °C for 24 h; the adsorption of the DPBF decreased from 0.50 to 0.43 (Figure 3e), which was consistent with the ¹H NMR data. In addition, the release of singlet oxygen from the PMMS-EPO at different temperatures is shown in Figure 3f. The release rate of singlet oxygen was clearly temperature-dependent, suggesting that the EPO could release singlet oxygen through thermal decomposition. The absorption of the DPBF showed neglectable decrease at 70 °C after 50 min, indicating that all of the stored singlet oxygen was released rapidly in 50 min. The purpose that we chose 70 °C was to know the decrease adsorption of the DPBF, when all of the stored singlet oxygen was consumed. Specifically, the singlet oxygen could be slowly released in the dark at body temperature (37 °C). The absorbance of the DPBF in the absence of PPMS-EPO/BPS at 25 °C and 70 °C had neglectable change, suggesting that the DPBF was stable even at 70 °C after 50 min (Figure S8a, Supporting

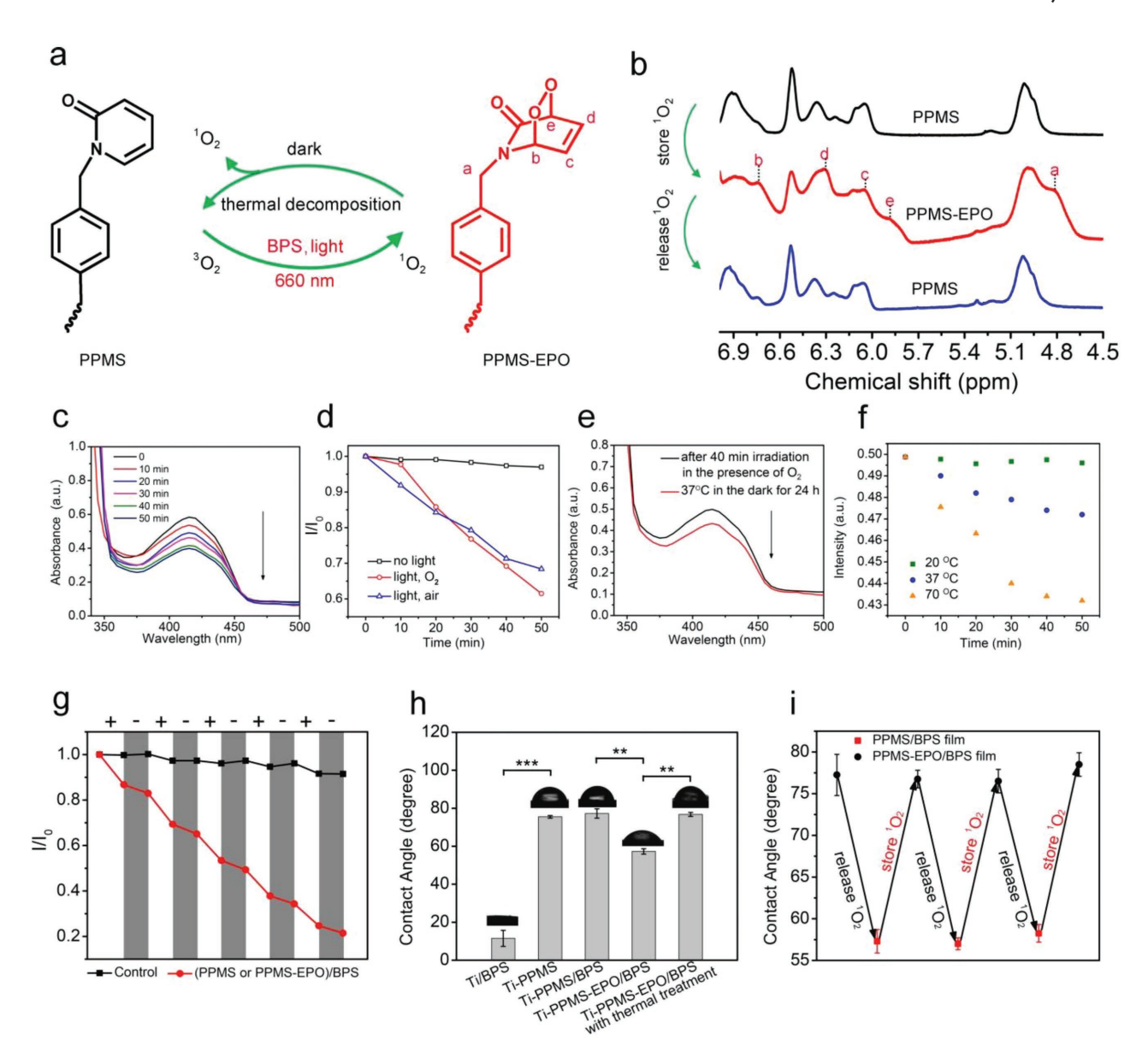


Figure 3. Storage, release, and detection of singlet oxygen. a) The operation mechanism of the reversible singlet oxygen storage (660 nm, 0.5 W cm⁻²) and release of PPMS and PPMS-EPO (dark, 37 °C). b) 1 H NMR spectra show the reversible structure change of PPMS and PPMS-EPO. c) UV–vis measurement of DPBF shows the singlet oxygen generation ability of PPMS/BPS with the increasing irradiation time in air at 20 °C (660 nm, 0.5 W cm⁻²). d) Normalized absorbance of the DPBF in the presence of PPMS/BPS in different conditions. e) The singlet oxygen released from PMMS-EPO/BPS after placing the sample in the dark at 37 °C for 24 h. f) Absorbance of the DPBF in the presence of PPMS-EPO/BPS at different temperature. g) Normalized absorbance of the DPBF in the presence of (PPMS or PPMS-EPO)/BPS and under light for 20 min (+, light cycles) or without light (-, dark cycles) at 70 °C for 50 min. The DMSO solution of DPBF without PPMS/EPO was served as control group. The two groups were bubbled with a gentle stream of oxygen in the light cycles. h) Contact angle of BPS, PPMS/BPS, PPMS-EPO/BPS, and PPMS-EPO/BPS with thermal treatment films. n = 3, **P < 0.01, ***P < 0.001. i) Reversible change of contact angle between PPMS/BPS and PPMS-EPO/BPS films after the storage and release of singlet oxygen for three times.

Information). Consequently, the PPMS/BPS was successfully endowed with generating singlet oxygen in the presence and absence of light.

To investigate the reversible storage and release of singlet oxygen from the PPMS/BPS, the PPMS/BPS in DMSO was treated with light (20 °C, 20 min) and dark (70 °C, 50 min) for five cycles. As depicted in Figure 3g, the decreased adsorption of DPBF was observed in both light and dark for five

cycles, indicating that this storage and release process could be repeated reversibly. As a control, the adsorption of DPBF without PPMS/BPS showed no significant change in the whole process. In addition, the surface wettability of samples on Ti substrates was measured by a contact angle (CA) system (Figure 3h). The CA of the BPS film was 11.5°, and it increased to 77.3° after being composited with PPMS, proving the hydrophobic property of PPMS. But this hydrophobic property can

only partially prevent the absorption of water. Some water still can enter into the film and cause the oxidation of the BPS surface. When the PPMS/BPS was converted to PPMS-EPO/BPS. the CA of the PPMS-EPO/BPS decreased to 57.3° due to the formation of an -O-O- bond. After placing the PPMS-EPO/ BPS film in the dark at 70 °C for 50 min, the CA turned back to 76.8°, suggesting that the PPMS-EPO/BPS thermally transformed into PPMS/BPS in the dark. After that, we studied whether the PPMS/BPS film could transform to PPMS-EPO/ BPS film reversibly. As above, the PPMS/BPS film in DMSO was treated with light (20 °C, 20 min) and dark (70 °C, 50 min) for three cycles. As illustrated in Figure 3i, the CA of the PPMS/BPS and PPMS-EPO/BPS films could change from around 77° to 57° reversibly for three cycles, further proving the repeatable storage and release of singlet oxygen from PPMS/BPS.

2.4. In Vitro Antibacterial Experiments

Benefiting from the singlet oxygen generation of PPMS/BPS in the presence and absence of light, the PPMS/BPS film could be used for antibacterial application. *Staphylococcus aureus* (*S. aureus*) (Gram-positive) and *Escherichia coli* (*E. coli*) (Gram-negative) were used to evaluate the antibacterial properties of (I) Ti, (II) Ti-PPMS/BPS, (III) Ti-PPMS-EPO/BPS, (IV) Ti+light, (V) Ti-PPMS/BPS+light, and (VI) Ti-PPMS-EPO/BPS+light. A spread plate method was used to evaluate the antibacterial

properties (Figure 4a-c). From Figure 4a-c, the (I) Ti and (II) Ti-PPMS/BPS groups showed similar bacteria viability, indicating the nontoxicity of Ti-PPMS/BPS in the dark. However, even without the irradiation of light, the (III) Ti-PPMS-EPO/ BPS group displayed significant increases in the antibacterial rate of 76.5% and 69.7% for E. coli and S. aureus, respectively. The antibacterial mechanism of Ti-PPMS-EPO/BPS was that singlet oxygen was stored in the film in the form of PPMS-EPO. The endoperoxide (EPO) group could be thermally decomposed slowly at 37 °C without light after 24 h and released singlet oxygen, which could be explained by the result of the singlet oxygen measurement (Figure 3e). Although the antibacterial rate did not reach above 90% due to limited stored singlet oxygen in films, but this antibacterial performance is enough for normal infection prevention. These results validate the assertion that singlet oxygen can be released from PPMS-EPO at 37 °C in the absence of light, killing most of the bacteria that adhered to the surface of the Ti-PPMS-EPO/BPS. After irradiation (660 nm light, 0.5 W cm⁻²) for 10 min, the (V) Ti-PPMS/BPS+light and (VI) Ti-PPMS-EPO/BPS+light groups could almost completely suppress the growth of bacteria; the antibacterial rate reached 97.5% and 99.3% against E. coli and 95.1% and 99.2% against S. aureus. The Ti-PPMS-EPO/ BPS+light group showed the greatest antibacterial ability, suggesting that a higher amount of singlet oxygen was generated from both the PPMS-EPO and BPS at 37 °C in the presence of light. Compared to the control group (IV) Ti+light, the light clearly had little influence on bacterial viability on the surface

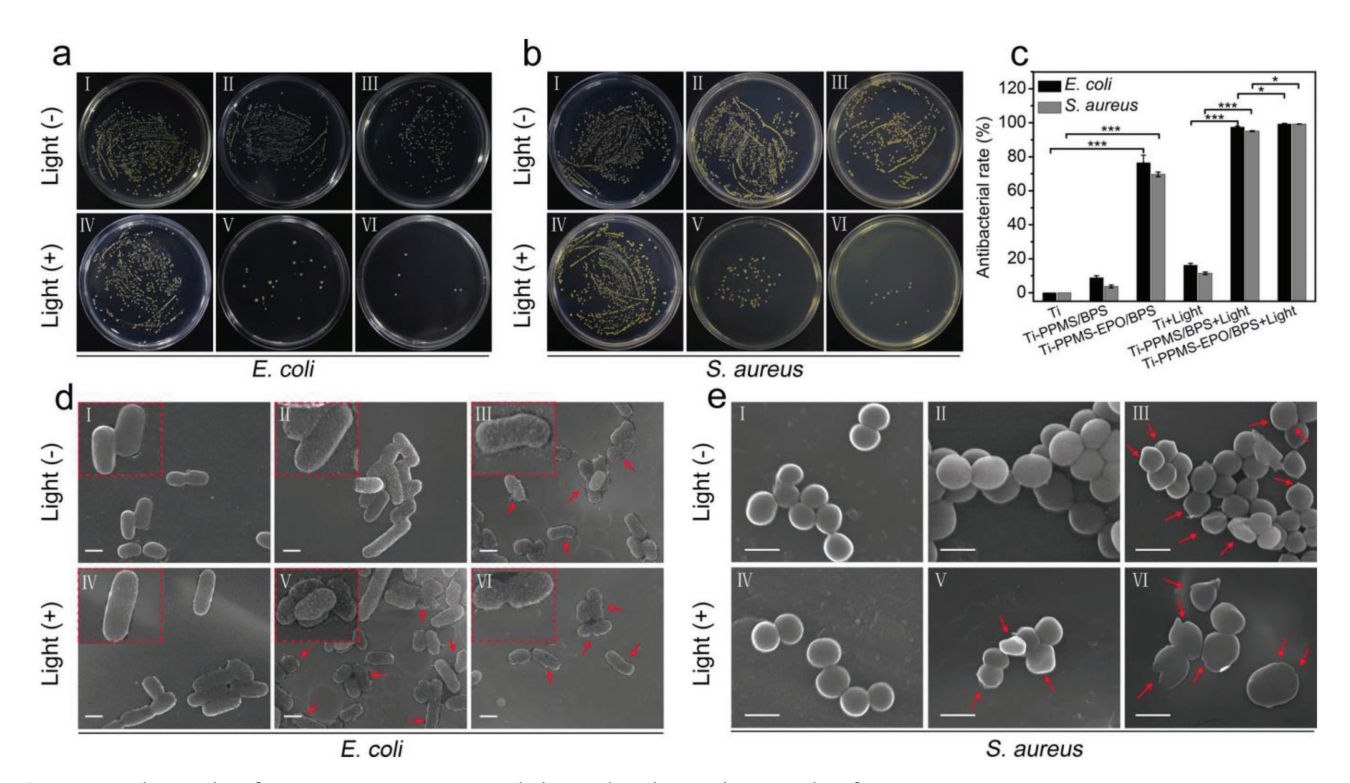


Figure 4. Antibacterial performance in vitro. a–c) Spread plate and antibacterial rate results of (I) Ti; (II) Ti-PPMS/BPS; (III) Ti-PPMS-EPO/BPS; (IV) Ti+light; (V) Ti-PPMS/BPS+light for *E. coli* and *S. aureus*, respectively. n=3, *P<0.05, ***P<0.001. d,e) SEM images of (I) Ti; (II) Ti-PPMS/BPS; (III) Ti-PPMS-EPO/BPS; (IV) Ti+light; (V) Ti-PPMS/BPS+light; (VI) Ti-PPMS-EPO/BPS+light for *E. coli* and *S. aureus*, respectively (scale bars, 1 μ m).





of the Ti. Also, the antibacterial rates had no obvious difference between group of Ti+light or only light, indicating that the light did not influence the viability of bacteria (Figure S9, Supporting Information). This result demonstrated the efficient bacteria-killing ability of the Ti-PPMS-EPO/BPS with or without light. To further investigate this antibacterial behavior, the morphology of the E. coli and S. aureus adhered to samples was observed by a SEM. For the E. coli (Figure 4d), the groups of (I) Ti, (II) Ti-PPMS/BPS, and (IV) Ti+light showed that the E. coli were typically rod shaped with integrated cell walls, indicating the samples' nontoxicity. In contrast, the rod shape of the E. coli became corrugated and distorted on the (III) Ti-PPMS-EPO/BPS, (V) Ti-PPMS/BPS+light, and (VI) Ti-PPMS-EPO/BPS+light surfaces (indicated by red arrows) since singlet oxygen could oxidize the lipid membrane and destroy the bacterial membranes.^[21] Similarly, compared to the regular spherical shape and integrated surface of S. aureus on the (I) Ti, (II) Ti-PPMS/BPS, and (IV) Ti+light groups, the cell walls of S. aureus had different degrees of shrinkage in the (III) Ti-PPMS-EPO/BPS group, and the shape became irregular in the (V) Ti-PPMS/BPS+light group. For the (VI) Ti-PPMS-EPO/ BPS+light group, the cell wall of the S. aureus was broken, and the S. aureus completely lost their cellular integrity; this high degree of damage was due to the increased singlet oxygen generated from the PPMS-EPO/BPS (Figure 4e). These results were consistent with those that were examined by spread plate. The bacteria viability was evaluated by the Live/Dead (green/red) staining assay and the corresponding fluorescent images were shown in Figure S10 (Supporting Information). Figure S10a,b (Supporting Information) showed that the numerous E. coli or S. aureus cells on the surfaces of the (I) Ti, (II) Ti-PPMS/ BPS, and (IV) Ti+light groups were stained green, indicating that these groups were nontoxic. Conversely, most bacteria were dead for the (III) Ti-PPMS-EPO/BPS and (V) Ti-PPMS/ BPS+light groups, and green spots were hardly observed in the (VI) Ti-PPMS-EPO/BPS+light group. The Live/Dead staining exhibited antibacterial trend results similar to the spread plate method and SEM examination. The antibacterial study showed that although some water or O2 was prevented from entering into the film, the efficient antibacterial photodynamic activity of BPS was not influenced.

2.5. In Vivo Antibacterial Assay

Since a 660 nm light source can be used to generate singlet oxygen for subcutaneous tumor treatment,^[22] we also evaluated the antibacterial ability of samples through photodynamic therapy in vivo, utilizing *S. aureus*-infected mice as the model animals. Before implantation, the *S. aureus* suspension (10⁷ CFU mL⁻¹, 20 μL) was dropped onto the surface of the above six groups and dried prior to implant. After suturing the surgery wound, the (IV), (V), and (VI) groups were irradiated with 660 nm light (0.5 W cm⁻²) toward the above samples for 20 min, respectively. The mice were sacrificed with an overdose of anesthetic. The surgery wounds were photographed with a digital camera (Figure S11, Supporting Information). The pictures showed that the (I) Ti, (II) Ti-PPMS/BPS, and (IV) Ti+light groups had some secretions due to

the inflammatory response of the tissue caused by *S. aureus*. In contrast, no secretions were found in the wounds of the (III) Ti-PPMS-EPO/BPS, (V) Ti-PPMS/BPS+light, and (VI) Ti-PPMS-EPO/BPS+light groups, indicating that the *S. aureus* was suppressed and the inflammatory response was relieved. To investigate the residue amount of *S. aureus* around the tissue and samples, the wound was washed with phosphate buffered saline (PBS) and the *S. aureus* was collected for the spread plate analysis. The spread plate results (**Figure 5**a) showed that the antibacterial rate of the (III) Ti-PPMS-EPO/BPS, (V) Ti-PPMS/BPS+light, and (VI) Ti-PPMS-EPO/BPS+light groups were 60.5%, 84.3%, and 98.2% compared to group (I), respectively.

To evaluate the bacterial infection of peri-implant soft tissues, hematoxylin and eosin (H&E) and Giemsa staining were employed (Figure 5b). The H&E staining showed typical signs of tissue infection in the (I) Ti, (II) Ti-PPMS/BPS, and (IV) Ti+light groups, including numerous necrotic cells, exudation, and neutrophil infiltration (indicated by red arrows) into tissues. Oedema of connective tissue and the loosening of collagenous fibers were observed in groups (I) and (II) (indicated by green arrows). However, the inflammatory reaction was markedly reduced in the (III) Ti-PPMS-EPO/BPS, (V) Ti-PPMS/ BPS+light, and (VI) Ti-PPMS-EPO/BPS+light groups. A slight inflammatory reaction in the (III) Ti-PPMS-EPO/BPS group was observed due to the slow release of singlet oxygen. In the (V) Ti-PPMS/BPS+light and (VI) Ti-PPMS-EPO/BPS+light groups, few inflammatory cells were observed, which resulted from the rapid disinfection of the samples under light. The 3-(4,5-dimethylthiazol-2-yl)-2,5-diphenyl-2Htetrazolium hydrobromide result showed that the (I) Ti, (II) Ti-PPMS/BPS, and (IV) Ti+light groups showed no cytotoxicity to MC3T3 cells, indicating the biocompatible of PPMS/BPS. Although the (III) Ti-PPMS-EPO/BPS, (V) Ti-PPMS/BPS+light and (VI) Ti-PPMS-EPO/BPS+light groups had obvious cytotoxicity in vitro (Figure S12, Supporting Information), the tissue around these samples exhibited little inflammatory reaction in vivo because the generated oxygen only killed the cells attached to the surface. Moreover, the amount of bacteria in the tissues of the (III) Ti-PPMS-EPO/BPS, (V) Ti-PPMS/BPS+light and (VI) Ti-PPMS-EPO/BPS+light groups also decreased significantly compared to the (I) Ti, (II) Ti-PPMS/BPS, and (IV) Ti+light groups. The degree of inflammatory reaction in the samples was consistent with the antibacterial behavior in vitro, and these results prove that the Ti-PPMS-EPO/BPS also exhibited substantial antibacterial performance with or without light in vivo. To investigate the antibacterial performance for long time in vivo, the bacteria were injected into the surface of Ti-PPMS/BPS at 7 d postsurgery. The antibacterial rate of Ti-PPMS/BPS+light was 92.8% compared to Ti-PPMS/BPS (Figure S13a, Supporting Information), suggesting that the photocatalytic performance of Ti-PPMS/BPS had negligible change at 7 d postsurgery due to the strengthened stability of BPS. Compared to the group of Ti-PPMS/BPS without light, the inflammatory reaction of Ti-PPMS/BPS+light was suppressed obviously (Figure S13b, Supporting Information). Finally, the histological analysis of liver, spleen, kidney, heart and lung of mice were performed by H&E staining at 7 d postsurgery. No signals of abnormalities or lesions of organ

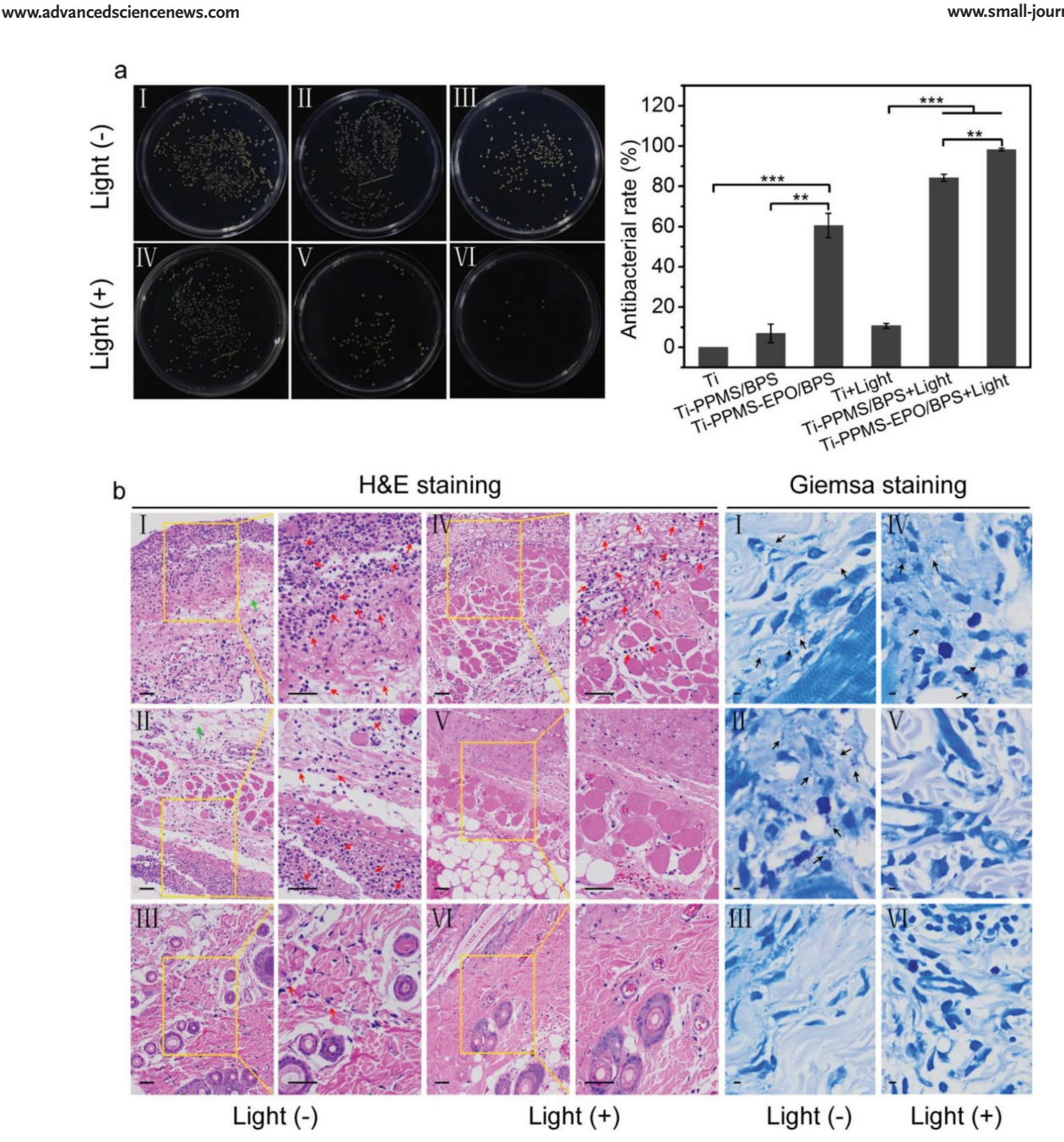


Figure 5. Antibacterial performance in vivo. a) Spread plate result and antibacterial rate of (I) Ti; (II) Ti-PPMS/BPS; (III) Ti-PPMS-EPO/BPS; (IV) Ti+light; (V) Ti-PPMS/BPS+light; (VI) Ti-PPMS-EPO/BPS+light. b) H&E (scale bars, 50 μ m) and Giemsa (scale bars, 10 μ m) staining images show tissue infection degree of samples. n=3, **P<0.01, ***P<0.001.

were observed, further demonstrating the excellent in vivo biocompatibility of this antibacterial film (Figure 6).

3. Conclusion

In summary, we have for the first time demonstrated a novel PDT antibacterial system based on BPS and PPMS that showed excellent antibacterial properties in the presence and absence of light. This system's mechanism not only effectively stores singlet oxygen in the form of PPMS-EPO produced from BPS

under the irradiation of 660 nm light but also releases it under thermal decomposition. This cycle of storing and releasing singlet oxygen is repeatable. The coprotection of hydrophobic PPMS and oxidation layer on the surface of BPS significantly suppressed the degradation of BPS. The ability to eliminate pathogen colonization in implant materials and on medical facility surfaces during, not just before, clinical use is a key improvement. This results of this study provided innovative and beneficial strategies for in situ rapid disinfection and preventing infection, and presented a new strategy to improve the stability of BPS.



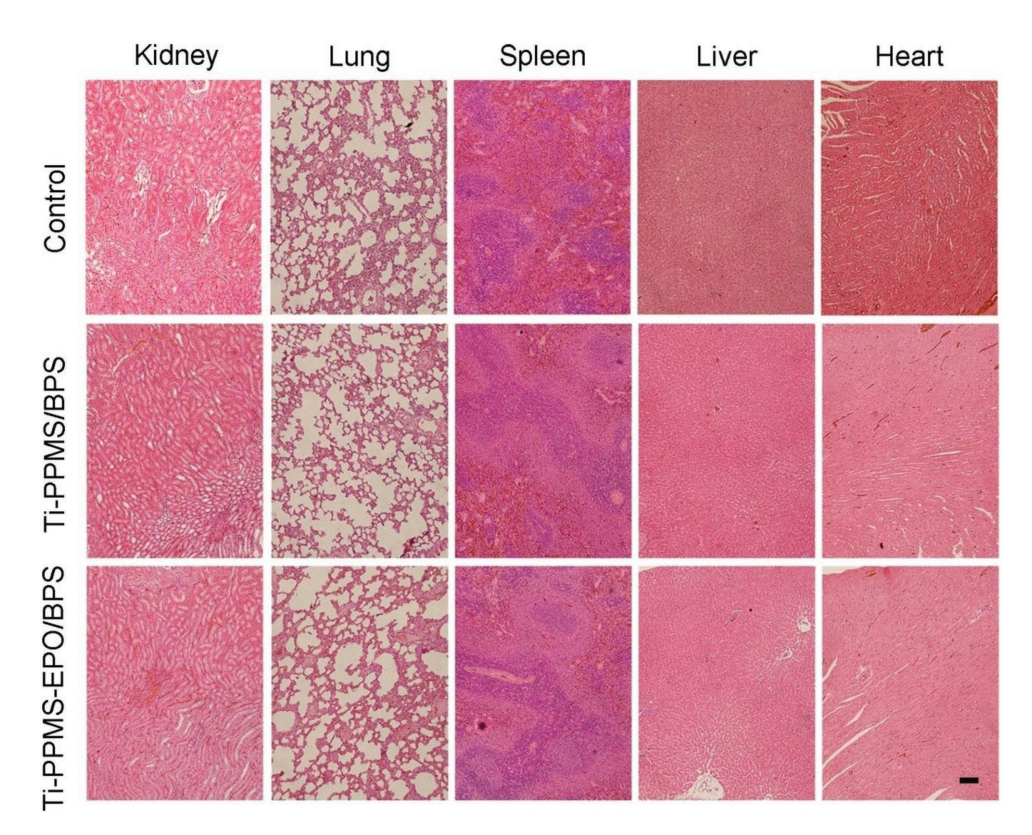


Figure 6. In vivo toxicity. H&E staining of heart, liver, spleen, lung, and kidney obtained from mice implanted with Ti-PPMS/BPS+light at 7 d postimplantation (scale bar, $100 \mu m$).

Supporting Information

Supporting Information is available from the Wiley Online Library or from the author.

Acknowledgements

L.T. and J.L. contributed equally to this work. This work was jointly supported by the National Natural Science Foundation of China, Nos. 51422102 and 81271715, and the National Key Research and Development Program of China, No. 2016YFC1100600 (subproject 2016YFC1100604), as well as Shenzhen Peacock Program (1108110035863317).

Conflict of Interest

The authors declare no conflict of interest.

Keywords

black phosphorus, chemical stability, disinfection, photodynamic, storage and release of $\ensuremath{\mathsf{ROS}}$

Received: September 15, 2017 Revised: October 21, 2017 Published online: December 18, 2017

- [1] D. M. A. Vera, M. H. Haynes, A. R. Ball, D. T. Dai, C. Astrakas, M. J. Kelso, M. R. Hamblin, G. P. Tegos, *Photochem. Photobiol.* 2012, 88, 499.
- [2] a) L. L. Ling, T. Schneider, A. J. Peoples, A. L. Spoering, I. Engels, B. P. Conlon, A. Mueller, T. F. Schaberle, D. E. Hughes, S. Epstein, M. Jones, L. Lazarides, V. A. Steadman, D. R. Cohen, C. R. Felix, K. A. Fetterman, W. P. Millett, A. G. Nitti, A. M. Zullo, C. Chen, K. Lewis, Nature 2015, 520, 455; b) C. Mao, Y. Xiang, X. Liu, Z. Cui, X. Yang, K. W. K. Yeung, H. Pan, X. Wang, P. K. Paul, S. Wu, ACS Nano 2017, 11, 9010; c) M. Li, X. Liu, Z. Xu, K. W. K. Yeung, S. Wu, ACS Appl. Mater. Interfaces 2016, 8, 33972; d) J. D. Rudolf, L. B. Dong, K. Manoogian, B. Shen, J. Am. Chem. Soc. 2016, 138, 16711; e) F. A. Mandl, V. C. Kirsch, I. Ugur, E. Kunold, J. Vomacka, C. Fetzer, S. Schneider, K. Richter, T. M. Fuchs, I. Antes, S. A. Sieber, Angew. Chem., Int. Ed. 2016, 55, 14852.
- [3] M. Baym, T. D. Lieberman, E. D. Kelsic, R. Chait, R. Gross, I. Yelin, R. Kishony, Science 2016, 353, 1147.
- [4] S. Rahimi, Z. T. Zadeh, M. A. K. Torshizi, R. Omidbaigi, H. Rokni, J. Agric. Sci. Technol. 2011, 13, 527.
- [5] a) E. D. Brown, G. D. Wright, Nature 2016, 529, 336; b) V. K. Sharma,
 J. Filip, R. Zboril, R. S. Varma, Chem. Soc. Rev. 2015, 44, 8410;
 c) M. F. Chellat, L. Raguz, R. Riedl, Angew. Chem., Int. Ed. 2016, 55, 6599; d) C. Marambio-Jones, E. M. V. Hoek, J. Nanopart. Res. 2010, 12, 1531; e) A. Besinis, T. De Peralta, C. J. Tredwin, R. D. Handy, ACS Nano 2015, 9, 2255.
- [6] Z. Hou, Y. Zhang, K. Deng, Y. Chen, X. Li, X. Deng, Z. Cheng, H. Lian, C. Li, J. Lin, ACS Nano 2015, 9, 2584.
- [7] a) X. Ragas, X. He, M. Agut, M. Roxo-Rosa, A. R. Gonsalves,
 A. C. Serra, S. Nonell, *Molecules* 2013, 18, 2712; b) W. S. Kuo,
 C. Y. Chang, H. H. Chen, C. L. L. Hsu, J. Y. Wang, H. F. Kao,
 L. C. S. Chou, Y. C. Chen, S. J. Chen, W. T. Chang, S. W. Tseng,





- P. C. Wu, Y. C. Pu, ACS Appl. Mater. Interfaces 2016, 8, 30467; c) C. Wang, Q. Cui, X Wang, L. Li, ACS Appl. Mater. Interfaces 2016, 8, 29101; d) J. Gehring, B. Trepka, N. Klinkenberg, H. Bronner, D. Schleheck, S. Polarz, J. Am. Chem. Soc. 2016, 138, 3076.
- [8] C. A. Robertson, D. H. Evans, H. Abraharnse, J. Photochem. Photobiol., B 2009, 96, 1.
- [9] a) E. Cabiscol, J. Tamarit, J. Ros, Int. Microbiol. 2010, 3, 3; b) P. Ma,
 H. Xiao, C. Yu, J. Liu, Z. Cheng, H. Song, X. Zhang, C. Li, J. Wang,
 Z. Gu, J. Lin, Nano Lett. 2017, 17, 928.
- [10] a) N. Nishiyama, Y. Morimoto, W. D. Jang, K. Kataoka, Adv. Drug Delivery Rev. 2009, 61, 327; b) W. Fan, P. Huang, X. Chen, Chem. Soc. Rev. 2016, 45, 6488.
- [11] M. Matsumoto, M. Yamada, N. Watanabe, Chem. Commun. 2005, 36, 483.
- [12] a) I. S. Turan, D. Yildiz, A. Turksoy, G. Gunaydin, E. U. Akkaya, Angew. Chem., Int. Ed. 2016, 55, 2875; b) D. Posavec, M. Zabel, U. Bogner, G. Bernhardt, G. Knor, Org. Biomol. Chem. 2012, 10, 7062.
- [13] a) H. Liu, A. T. Neal, Z. Zhu, D. Tománek, P. D. Ye, ACS Nano 2014, 8, 4033; b) L. Li, J. Kim, C. Jin, G. Ye, D. Y. Qiu, F. H. da Jornada, Z. Shi, L. Chen, Z. Zhang, F. Yang, K. Watanabe, T. Taniguchi, W. Ren, S. G. Louie, X. Chen, Y. Zhang, F. Wang, Nat. Nanotechnol. 2017, 12, 21.
- [14] a) H. Wang, X. Yang, W. Shao, S. Chen, J. Xie, X. Zhang, J. Wang, Y. Xie, J. Am. Chem. Soc. 2015, 137, 11376; b) R. Lv, D. Yang, P. Yang, J. Xu, F. He, S. Gai, C. Li, Y. Dai, G. Yang, J. Lin, Chem. Mater. 2016, 28, 4724.

- [15] a) Y. Zhao, H. Wang, H. Huang, Q. Xiao, Y. Xu, Z. Guo, H. Xie, J. hao, Z. Sun, W. Han, X. F. Yu, P. Li, P. K. Chu, Angew. Chem., Int. Ed. 2016, 55, 5003; b) B. Yang, B. Wan, Q. Zhou, Y. Wang, W. Hu, W. Lv, Q. Chen, Z. Zeng, F. Wen, J. Xiang, S. Yuan, J. Wang, B. Zhang, W. Wang, J. Zhang, B. Xu, Z. Zhao, Y. Tian, Z. Liu, Adv. Mater. 2016, 28, 9408; c) G. Abellan, V. Lloret, U. Mundloch, M. Marcia, C. Neiss, A. Gorling, M. Varela, F. Hauke, A. Hirsch, Angew. Chem., Int. Ed. 2016, 55, 14557.
- [16] D. Hanlon, C. Backes, E. Doherty, C. S. Cucinotta, N. C. Berner, C. Boland, K. Lee, A. Harvey, P. Lynch, Z. Gholamvand, S. Zhang, K. Wang, G. Moynihan, A. Pokle, Q. M. Ramasse, N. McEvoy, W. J. Blau, J. Wang, G. Abellan, F. Hauke, A. Hirsch, S. Sanvito, D. D. O'Regan, G. S. Duesberg, V. Nicolosi, J. N. Coleman, *Nat. Commun.* 2015, 6, 8563.
- [17] J. Shao, H. Xie, H. Huang, Z. Li, Z. un, Y. Xu, Q. Xiao, X. Yu, Y. Zhao, H. Zhang, H. Wang, P. K. Chu, Nat. Commun. 2016, 7, 12967.
- [18] H. U. Lee, S. C. Lee, J. Won, B. C. Son, S. Choi, Y. Kim, S. Y. Park, H. S. Kim, Y. C. Lee, J. Lee, Sci. Rep. 2015, 5, 8691.
- [19] C. Hao, B. Yang, F. Wen, J. Xiang, L. Li, W. Wang, Z. Zeng, B. Xu, Z. Zhao, Z. Liu, Y. Tian, Adv. Mater. 2016, 28, 3194.
- [20] C. J. Shih, S. Lin, M. S. Strano, D. Blankschtein, J. Am. Chem. Soc. 2010, 132, 14638.
- [21] Y. Tao, E. G. Ju, J. Ren, X. Qu, Adv. Mater. 2015, 27, 1097.
- [22] a) G. F. Luo, W. H. Chen, Q. Lei, W. X. Qiu, Y. X. Liu, Y. J. Cheng, X. Z. Zhang, Adv. Funct. Mater. 2016, 26, 4339; b) H. Cheng, J. Y. Zhu, S. Y. Li, J. Y. Zeng, Q. Lei, K. W. Chen, C. Zhang, X. Z. Zhang, Adv. Funct. Mater. 2016, 26, 7847.